Enhanced simulation of the bowed cello string

Hossein Mansour
CIRMMT, CAML
Schulich School of Music
McGill University
Montreal, Québec H3A 1E3, Canada
hosse-in.mansour@mail.mcgill.ca

Jim Woodhouse
Cambridge University Engineering Department
jw12@cam.ac.uk

Gary P. Scavone
CIRMMT, CAML
Schulich School of Music
McGill University
Montreal, Québec H3A 1E3, Canada
gary@music.mcgill.ca

ABSTRACT

A detailed time-domain simulation is implemented to model the bowed cello string. Building on earlier simulation models [1-3], several new features have been added to make the model more realistic. In particular, a large number of body modes, both transverse polarizations of the string motion, the longitudinal vibrations of the bow hair and the effect of the sympathetic strings are included. These additional features can be turned on and off in the model to evaluate their relative importance. To the best of our knowledge this is the first time that the second polarization of the string and the effect of the sympathetic strings have been included in a bowed-string simulation. The compliance of the bow-hair was accounted for in previous studies but without considering its own vibration properties [4]. Different features of the model are turned on and the classic Schelleng minimum bow-force [5] is calculated for combinations of bow-bridge distance and different notes being played on the string. The main finding is that all features reduce the minimum bow-force to some extent. This reduction is almost frequency independent for the case of the second polarization and the longitudinal bow-hair vibration, but clearly frequency-dependent for the sympathetic strings case.

1. INTRODUCTION

The time-domain simulation of the bowed string has been the subject of many studies in recent years and as a result, many features of bowed strings have been explained qualitatively and to a certain extent quantitatively [6, 7]. Different mechanical details of the bowed string have previously been investigated in the hope of making the numerical models match the experimental measurements over a wide range of bowing gestures of musical interest. Among those details added to the model are torsional vibration of the string [8], bending stiffness of the string [9], effect of a close body resonance resulting in a "wolf note" [1], longitudinal bow-hair compliance [4], and the effect of the bow's finite width [2]. This study is aimed at adding more such details to the model. Specifically, modal properties of the body, dual-polarization of the string, longitudinal vibration of the bow-hair, and the effect of the sympathetic strings are taken into account.

2. MATERIAL AND METHOD

2.1 Basic model of the bowed string

The simulation results in this paper are based on modeling the best-understood musical string, a cello *D* string (Thomastik 'Dominant'). For this particular string a reasonably complete set of calibration data is available, covering transverse vibration frequencies and damping factors, torsional frequencies and damping factors, and bending stiffness. In short, the characteristic impedance of the string in the transverse direction is $Z_D = 0.55$ Ns/m and a constant Q-factor of 500 is assumed and implemented in the reflection functions using the method proposed in [8], which only reflects the intrinsic damping of the string. The reflection functions from the bridge side and the finger side are modified as suggested in [9], to take into account wave dispersion due to the bending stiffness of the strings. The string tension, bending stiffness, and cutoff frequency [9] were respectively 111 N, $3\text{x}10^{-4}$ Nm^2, and $3\text{x}10^4$ Hz. Torsional vibrations are also taken into account and parameters were extracted from [8]. The torsional wave has the characteristic impedance of 1.8 Ns/m, constant Q-factor of 45, and propagation speed of 1060 m/s. The position of the bowed point on the string is denoted by the dimensionless quantity β, which is the fractional distance of the bow from the bridge (i.e. $\beta = \frac{\text{bow–bridge distance}}{\text{string length}}$). The time-step used for all simulations is $5\text{x}10^{-6}$ second.

All simulations of this study are done using the old velocity dependent friction model (also known as Friedlander's friction curve [10]) whose parameters are extracted from the constant slipping experiments reported in [11]. Although now known to be wrong in some respects, the friction-curve model has been so far remarkably successful in describing, at least qualitatively, many observed aspects of bowed-string behavior [3]. The physically more accurate visco-plastic friction model is more computationally demanding, and still involves unresolved research questions for its details [12]. Incorporating such a model is a topic for future research.

2.2 Model of the body

Calibrated measurements have been made on the *C*-string corner of two mid-quality cellos. A miniature hammer (PCB Model 086E80) and LDV (Polytec LDV-100) were used to make the full set of measurements in the bowing plane (i.e. X-X, Y-Y, X-Y, and Y-X where X represents

the bowing direction and Y is the direction normal to that in the bowing plane).

Compensation for the strings is made as described in [13] such that the admittances are adjusted to account for all strings. For a cello, each string has a vibrating length on both sides of the bridge, so that if all of these are damped then the sum should be taken over eight semi-infinite strings. Equation (1) is used to deduce $Y_{\mathrm{body}}(\omega)$ from the measured $Y(\omega)$.

$$\frac{1}{Y(\omega)} = \frac{1}{Y_{\mathrm{body}}(\omega)} + \sum_j Z_j \qquad (1)$$

Since both polarizations of the strings are taken into account, each admittance matrix (i.e. $Y_{\mathrm{body}}(\omega)$ and $Y(\omega)$) is a 2x2 ideally symmetric matrix and $\sum_j Z_j$ in Equation (1) can be calculated as:

$$\sum_j Z_j = \left(\sqrt{\rho_{\mathrm{C}} T_{\mathrm{C}}} + \sqrt{\rho_{\mathrm{G}} T_{\mathrm{G}}} + \sqrt{\rho_{\mathrm{D}} T_{\mathrm{D}}} + \sqrt{\rho_{\mathrm{A}} T_{\mathrm{A}}}\right) \begin{bmatrix} 1 & 0 \\ 0 & 1 \end{bmatrix}, \qquad (2)$$

where indices *C*, *G*, *D*, and *A* represent the different strings of the cello, ρ is the density of the strings with units kg/m and *T* is the tension of the strings.

As discussed in [13], using Equation (1) will result in the admittances being compensated too generously since the strings cannot be perfectly damped with conventional damping methods. As expected, adding the compensation to the admittances has resulted in sharper peaks with higher Q-values.

Consequently, for Cello #1, which is used the most in the simulations, 89 modes were used to synthesize the admittance up to the frequency of 5 kHz; among these, 8 were below 100 Hz. Those low frequency modes were included in the curve fitting process to keep their residual effect, but were later removed from the simulations as any relative bridge-corpus motion is unlikely over that low frequency range. The curve fitting process was performed using ME'Scope, a commercial modal analysis package. Top priority was given to fit the X-X admittance as precisely as possible, the second priority was given to fitting the X-Y (or alternatively Y-X) data, and finally the Y-Y admittance was reconstructed according to the parameters enforced by X-X and X-Y and Equations (3) repeated from [14]. The measured admittances and their reconstructions are compared in Figure 1.

$$Y_{\mathrm{xx}}(\omega) = \sum_k \frac{\mathrm{i}\omega \cos^2\theta_k}{m_k(\omega_k^2 - \mathrm{i}\omega\omega_k/Q_k - \omega^2)} \qquad (3.1)$$

$$Y_{\mathrm{yy}}(\omega) = \sum_k \frac{\mathrm{i}\omega \sin^2\theta_k}{m_k(\omega_k^2 - \mathrm{i}\omega\omega_k/Q_k - \omega^2)} \qquad (3.2)$$

$$Y_{\mathrm{xy}}(\omega) = Y_{\mathrm{yx}}(\omega) = \sum_k \frac{\mathrm{i}\omega \cos\theta_k \sin\theta_k}{m_k(\omega_k^2 - \mathrm{i}\omega\omega_k/Q_k - \omega^2)} \qquad (3.3)$$

The final result of the reconstruction is four 81-element vectors containing the natural frequencies, Q-factors, modal masses (*m*), and mode angles (θ) that were fed into the bowed-string model. The same procedure was applied to the measurements made on Cello #2 with a slightly different number of modes. It is noteworthy that θ indicates the angle between the principal direction of vibration for each mode with respect to the bowing direction. This angle is deduced from the relative expression of each mode in the measured admittances of different directions (calculated from Equations (3.1) to (3.3)).

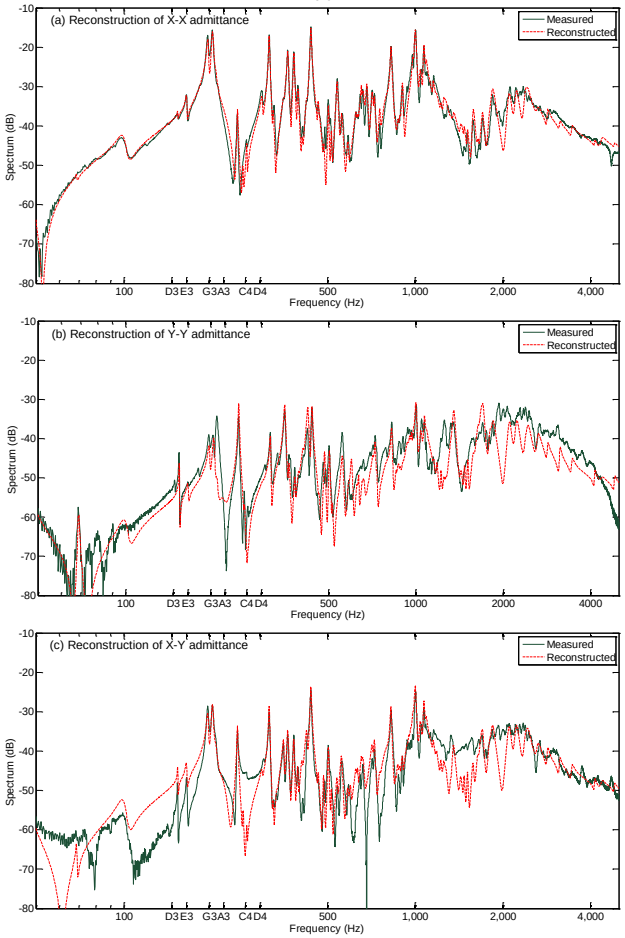

Figure 1: Measured admittances on the C-string side of the cello (solid green line) together with their reconstruction with 81 modes (dashed red line). X represents the bowing direction and Y direction is perpendicular to that. (a) X-X measurement, (b) Y-Y and (c) X-Y (or alternatively Y-X); for easier comparison some musical scales are also shown on X-axis.

The body modes are included in the bowed-string model using an IIR technique described in [14]. The time step used in our simulations allows for 40 time-samples in each period of the highest simulated body mode. Each (k^{th}) mode is modeled as an independent resonator and its damped free oscillation is modified by the value $F_{\mathrm{Excit}}(k) * h/m_k$ in each time step where *h* is the time step and $F_{\mathrm{Excit}}(k)$ is the instantaneous force applied by the string(s), projected in the principal direction of mode *k*.

F_{Excit} itself is a function of the incoming wave velocities from the bowed string in the X and Y directions (V_{Xin} and V_{Yin}) as well as the velocity of the bridge notch in the *X* and *Y* directions (V_{XBridge} and $V_{YBridge}$) which can be approximated by their value at the previous time step as:

$$V_{\mathrm{XBridge}} = \Re e\left\{\sum_k A_{k(\mathrm{Bridge})} \cos(\theta_k)\right\} \qquad (4.1)$$

$$V_{YBridge} = \Re e\left\{\sum_k A_{k(\mathrm{Bridge})} \sin(\theta_k)\right\}, \qquad (4.2)$$

where $A_{(\mathrm{Bridge})}$ is the complex vector of mode velocities. F_{Excit}, the vector of modal forces, can thus be calculated from

$$F_{\mathrm{Excit}} = 2 * Z_D * (V_{\mathrm{Xin}} * \cos\theta + V_{\mathrm{Yin}} * \sin\theta) - 2 * \left(V_{\mathrm{XBridge}} * \cos\theta + V_{\mathrm{YBridge}} * \sin\theta\right) * (Z_{\mathrm{D}} + Z_{\mathrm{C}} + Z_{\mathrm{G}} + Z_{\mathrm{A}}), \quad (5)$$

which will reduce to the form of Equation (6) if we only consider a single polarization of the string (i.e. the bowing direction):

$$F_{\mathrm{Excit}} = 2 * Z_{\mathrm{D}} * V_{\mathrm{Xin}} * \cos\theta - 2 * V_{\mathrm{XBridge}} * \cos\theta * (Z_{\mathrm{D}} + Z_{\mathrm{C}} + Z_{\mathrm{G}} + Z_{\mathrm{A}}). \quad (6)$$

In both Equations (5) and (6) the first term corresponds to the reaction force of the bridge resulting in the phase reversal of the reflected velocity wave of the bowed string and the second term allows for the fact that movement of the bridge sends out velocity waves in all strings whether the strings are damped or not and regardless of the amount of incoming velocity wave from the strings. It is noteworthy that this effect was accounted for when the admittance was being measured with the strings damped but was taken out later by admittance compensation. The factor of two for the first term represents the difference of the incoming and outgoing waves and for the second term relates to the fact that a cello has strings extending on both sides of the bridge (as opposed to a guitar for example).

2.3 Second polarization of the string

The movement of the bridge notch is not necessarily in the bowing direction for all body modes. Also, the bow-hair is not rigid enough to suppress all the string vibrations normal to it. As shown in Equation (5), the X and Y polarizations of the bowed-string are coupled together via the bridge. Incoming waves in the X and Y directions add up to excite modes that are not necessarily lined up in either direction. Projected velocities of each mode in the X and Y directions ($V_{\mathrm{XBridge}}(k)$ and $V_{\mathrm{YBridge}}(k)$) add, consequently, to the reflected waves at the bridge.

In this regard, the bow-hair needs to be flexible in its transverse direction to allow for this second polarization of the string motion. A pair of traveling waves is considered to model this bow hair transverse vibration. The bow hair ribbon is assumed to have mass per unit length 0.0077 kg/m, length 0.65 m and total tension 60 N [15]. A Q-factor of 20 is used for the transverse waves as estimated in [16]. This will result in a fundamental of 68 Hz for bow-hair vibrations in the transverse direction. The "bow β" (distance from the contact point to the frog divided by the full length of the hair ribbon) is arbitrarily chosen to be 0.31 which does not change during the simulation as its dynamics are assumed to be much slower than the dynamics of the string itself.

The transverse vibration of the bow-hair is excited by the normal-to-bow vibrations of the string; hence the bow and the string are coupled at the contact point. The constraint at the contact point is that they share a common velocity and apply the same amount of force to each other in opposite directions. To find the unknown common velocity and the mutual force, the velocity of the string and the bow are first calculated in the absence of the other one. These values, called V_{Yh} and V_{bTh}, represent history of the string velocity in the *Y* direction and history of the bow-speed in the transverse direction. With simple math it can be shown that the matched velocity (V_{match}) will be equal to

$$V_{\mathrm{match}} = \frac{V_{\mathrm{Yh}} * Z_{\mathrm{D}} + V_{\mathrm{bTh}} * Z_{\mathrm{bT}}}{Z_{\mathrm{D}} + Z_{\mathrm{bT}}} \quad (7)$$

and the resulting fluctuating force in the contact region (F_{fluc}) will be

$$F_{\mathrm{fluc}} = 2 * Z_{\mathrm{D}} * (V_{\mathrm{match}} - V_{\mathrm{Yh}}). \quad (8)$$

This force is added to the nominal value of the bow-force, supplied by the player, to give the effective bow-force as in Equation (9). Since the bow-force is being dynamically updated for each time step, the friction curve should consequently be re-scaled.

$$F_{\mathrm{eff}} = F_{\mathrm{nom}} + F_{\mathrm{fluc}} \quad (9)$$

2.4 Longitudinal bow-hair vibration

Bow-hair also has some degree of compliance in the longitudinal direction, which is excited by the fluctuating friction force between the bow and the string. The characteristic impedance of the hair ribbon in the longitudinal direction (called Z_{bL}) is about 10 Ns/m [4]; the wave speed in the longitudinal direction 2300 m/s [15]; and the Q-value approximated at 10 [16]. In the presence of bow-hair longitudinal vibrations, the nominal bow velocity will be modulated by the velocity of the contact point on the bow-hair relative to the bow stick. This relative velocity can be found from:

$$V_{\mathrm{bFluc}} = V_{\mathrm{L\_intip}} + V_{\mathrm{L\_infrog}} + \frac{F_{\mathrm{f}}}{2 * Z_{\mathrm{bL}}} \quad (10)$$

and the effective bow speed can be calculated from

$$V_{\mathrm{bEff}} = V_{\mathrm{b}} - V_{\mathrm{bFluc}}\,, \quad (11)$$

where F_{f} is the instantaneous friction force between the bow and the string, V_{b} is the nominal bow speed provided by the player, and $V_{\mathrm{L\_intip}}$ and $V_{\mathrm{L\_infrog}}$ are the incoming longitudinal velocity waves, from the tip and the frog respectively, arriving at the contact point. It is noteworthy that since the friction curve is a function of bow speed, it should be reconstructed with V_{bEff} instead of V_{b} at each time step.

The effect of the bow-stick modes was also taken into account elsewhere [17]. Briefly, the interaction of the longitudinal and transverse bow-hair vibration with the stick modes can be implemented in a similar fashion to the string's dual polarization motion with the body modes. The effect of the bow-stick modes was, however, negligible when compared to the effect of the transverse and longitudinal vibrations of the bow-hair itself.

2.5 Sympathetic strings

Under normal playing conditions the bow continuously excites one string and the other three are free to vibrate, their excitation being provided by the moving bridge. This certainly has an effect on the playability of a note, particularly when one or more of the coupled strings have harmonics matching those of the bowed string.

Physical properties of those three strings were extracted from [18] and their vibrations are simulated using the same method as for the bowed string. Only a single polarization is considered for the sympathetic strings; however, their resistance against bridge vibration in the *Y* direction is also taken into account. The single polarization assumption is made based on the fact that most of the

body modes in the lower range of frequencies result in a rocking motion of the bridge which is approximately in the *X* direction for all strings. Based on the same assumption, a single body admittance is used for all four strings. Equation (12) shows the modified version of Equation (5) for the case with sympathetic strings:

$$F_{\text{Excit}} = 2 * Z_{\text{D}} * ((V_{\text{Xin}} - V_{\text{XBridge}}) * \cos\theta + (V_{\text{Yin}} - V_{\text{YBridge}}) * \sin\theta) + \sum_{\text{j=C,G,A}} 2 * \text{Z}_j * (V_{j\text{in}} * \cos\theta - V_{\text{XBridge}} * \cos\theta - V_{\text{YBridge}} * \sin\theta) \quad (12)$$

The single polarization assumption results in an underestimate of the sympathetic strings' effect.

2.6 Summary of the model

The model of the bowed string allows for up to 6 different types of motion, each of which is modeled with a pair of superposed traveling waves: 1) vibration of the bowed string in the bowing direction; 2) vibration of the bowed string in the direction perpendicular to the bow; 3) torsional vibration of the string; 4) transverse vibration of the bow-hair; 5) longitudinal vibration of the bow-hair, and 6) single polarization vibrations of the three sympathetic strings. It also uses 81 independent resonators to simulate body modes. The code adjusts the effective length of the bowed string based on the chosen fundamental frequency.

3. RESULTS AND DISCUSSION

Different combinations of the above mentioned degrees of freedom are allowed and their relative importance can be evaluated. Schelleng maps are calculated for each case to see the effect on the playability of the cello. Schelleng calculated formulae for the maximum and minimum bow-forces between which the Helmholtz motion of the string is possible, and plotted the results in the plane of force against bowing position on a log-log scale [19]. The following simulations are made on the first 13 semi-tones played on the D string, giving the possibility to study the note-by-note variations of the instrument. Each map studied in this paper is composed of a grid of 7800 time-domain simulations, each 1 s long. The grid is formed by different combinations of the played note, β, and bow-force (20 values for β and 30 values of bow force, all exponentially spaced). β ranged from 0.02 to 0.22 and force ranged from 0.0005 N to 2.5 N. The bow velocity was chosen to be 0.05 m/s in all cases, although varying that value might form an interesting study in its own right [19]. Motion of the string in the bowing direction was always initialized with a proper sawtooth wave. In all cases torsional vibration of the string and its bending stiffness were taken into account. Each time domain waveform is automatically classified into Helmholtz, double slip, constant slipping, ALF [20] and Raman higher types [21] using the method proposed in [3] and modified in [12]. A separate function automatically calculates the minimum bow-force for each combination of played note and β. The result is a surface similar to the one shown in Figure 2. Slices of this surface in the frequency and β directions are comparable to the lower limit of the classic Schelleng diagram and to a sampled version of the minimum bow-force proposed in [22]. Another interesting possibility with this 3-D Schelleng diagram is to find the geometric mean of the minimum bow-force when averaged over frequency or over β to see more global effects (see for example Figure 3).

3.1 The body effect

The minimum bow-force surface for Cello #1 is plotted in Figure 2. As was expected from the admittance, a mountain range is observed from *F#* to *G#*. To study the influence of body modes on minimum bow force the same plot is calculated for our second studied cello (called Cello #2). The results averaged over frequency and over β are compared for the two instruments in Figures 3a and 3b respectively. The average over β (Figure 3a) shows that these two instruments behave slightly differently on different notes, specially in the wolf range, but the average over frequencies (Figure 3b) shows that these differences are mostly local and neither of the two instruments is globally more "playable" in this sense than the other. The β averaging is taken over the first 13 exponentially spaced β values ranging from β = 0.02 to β = 0.09; beyond β = 0.1 or so, the minimum bow-force is mostly driven by string properties and Helmholtz usually breaks down to constant slipping with no sign of double slip. For the same reason, Figure 3b is only plotted up to β=0.117.

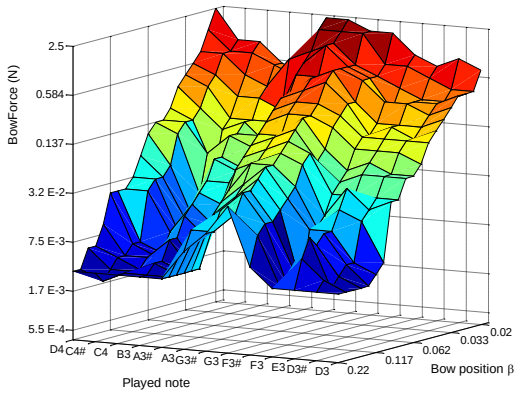

Figure 2: Minimum bow-force as a function of played note and β for Cello #1. Only the body is included in the model and all other options are turned off.

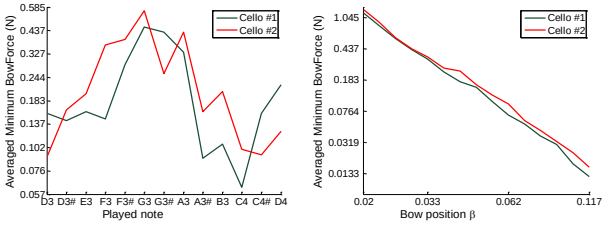

(a) (b)

Figure 3: Minimum bow-force for Cellos #1 and #2 averaged over β (a), and over thirteen semitones of D3 to D4 (b). The instrument is being played with a rigid bow, and the other strings are damped

It is expected to see a stronger effect of body for the *C* string due to its closer impedance match to the body. However, no effort was made to simulate such effect in this study as the full mechanical properties of the *C* string were not available as much as they were for the *D* string.

3.2 Dual string polarization

The effect of the second string polarization together with compliant bow-hair in the transverse direction is studied in this section. Adding the second polarization can potentially affect the playability of the instrument in two ways: a) by modulating the effective bow-force according to Equation (9) and b) by absorbing energy from the string and damping the transients/disturbances that can potentially trigger a second, premature slip. The latter effect can only reduce the effective bow-force while the former can either increase or decrease it depending on the relative phase of bow-hair and stick-slip motions.

It can be seen from Figure 4 that the second string polarization has generally reduced the effective bow-force. The effect is even more visible for larger βs in Figure 4b. A possible explanation for this β dependency is that the amplitude of string vibration in both polarizations gets higher when the bow moves farther from the bridge, thus a stronger string-bowhair coupling can occur.

An interesting observation in Figure 4a is that the bow-force reduction is almost independent of the note being played. The fundamental frequency of the bow-hair in the transverse direction is around 68 Hz, so one may expect a further minimum bow-force reduction in integer multiples of this frequency (i.e. *G3#*, *C4#*). This did not happen, for two possible reasons: a) the bow-β used in this simulation is close to 1/3 and thus the third mode of the bow-hair can not contribute much; b) the bow-hair is heavily damped (Q=20), so fairly broad peaks are expected in the impedance of the bow-hair, which cannot create a strong frequency-dependent behavior (this agrees with the experience of the players that the playability of a particular instrument is not strongly dependent on bow tension or bow-β). Of course, a stronger frequency dependency may be expected if a strong body resonance with a mode angle close to 45° exists close to one of the played notes.

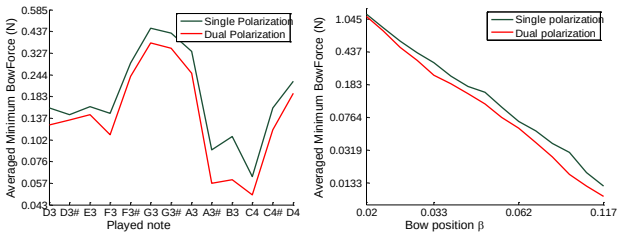

(a) (b)

Figure 4: Effect of the second string polarization on the minimum bow-force of Cello #1, averaged over β (a), and over thirteen semitones of *D3 to D4* (b). In both plots the green line is for the single polarization (same as Green in Figure 3.a and 3.b) and the red is for dual string polarizations

3.3 Longitudinal bow-hair vibration

The effect of the longitudinal bow-hair vibration on the minimum bow-force is plotted in Figures 5a and 5b. As can be seen, the only difference is a slight reduction, which is probably due to a small energy absorption from the string. The insignificance of this effect can probably be traced to the large impedance mismatch between the bow-hair in the longitudinal direction (around 10 Ns/m) and the string in the transverse direction (0.55 Ns/m). A much stronger effect was observed when the bow-hair characteristic impedance was reduced to 4 Ns/m. Also a stronger effect might be expected when studying faster transients of the string such as the ones studied in [23].

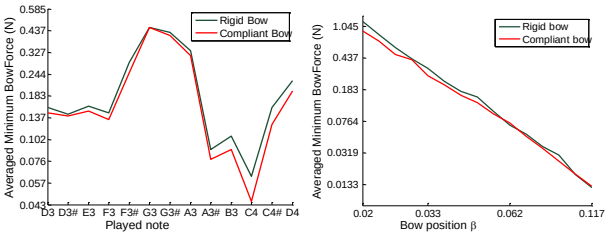

(a) (b)

Figure 5: Effect of the longitudinal bow-hair vibration on the minimum bow-force of Cello #1, averaged over β (a), and over thirteen semitones of *D3 to D4* (b). In both plots the green line is for a rigid bow (same as Green in Figure 3.a and 3.b) and the red is for a bow compliant in longitudinal direction

Another interesting observation from the grid of classified motions is more frequent occurrence of ALF notes when longitudinal bow-hair vibration was allowed. For the simulations over the *D3* to *D4* octave, 102 ALF occurrences were observed for a compliant bow as compared to 62 for a rigid bow. This point was emphasized by Mari Kimura in [24] *"The first secret is maintaining loose bow-hair…. You don't want a lot of tension… You need enough elasticity on the bow-hair that you can really grab the string."*

3.4 The sympathetic strings

The effect of three sympathetic strings is systematically studied in this section. An octave range is played on the *D* string of Cello #1 and the resulted minimum bow-force is compared for the cases of damped and undamped sympathetic strings (with a regular *C-G-D-A* tuning). The exact effect is somehow complicated (see [25] section 5) and needs further analysis but the general expectation would be a reduction in the minimum bow-force when one or more of the coupled strings are sympathetically tuned with the played note. In this regard, four notes in the octave *D3* to *D4* are expected to be affected:

- *G3* which is an octave above *G2* (twice the frequency) and an octave and a fifth above *C2* (three times in frequency)
- *A3* that is unison with the *A3* coupled string
- *C4* which is two octaves above *C2* (four times the frequency)
- *D4* which is an octave and a fifth above *G2* (three times the frequency)

This effect is clearly visible in Figure 6a. A consistent "deep canal" can be seen on *G3* which has support from two coupled strings and also happens to be around the strongest body resonance represented by a mountain range in Figure 2.

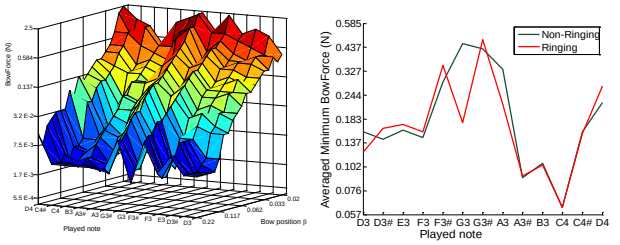

(a) (b)

Figure 6: Minimum bow-force as a function of played note and β for Cello #1 similar to Figure 2 but being played when the other three strings were free to vibrate (a); β-averaged minimum bow-force with and without the sympathetic strings (b)

It is more revealing to look at the β-averaged minimum bow-force with and without the sympathetic strings (Figure 6b). A similar effect is observed for *A3* to a lesser extent; however, *C3* and *D4* were not much affected by the sympathetic strings. A possible explanation for the *C3* case is that its minimum bow-force was already quite low without the sympathetic strings; thus its dynamics are most likely being driven by the intrinsic damping of the string itself rather than the vibrations of the bridge. *D4*'s independency on the sympathetic strings might be associated with the fact that it only gets support from every third partial of *G2*, which are apparently not so effective.

4. CONCLUSIONS

New features have been added to the model of the bowed string. A detailed body model is implemented whose parameters were extracted from calibrated admittance measurements. The model takes into account the angle of body modes with respect to the bowing direction, which transforms the initial excitation of the string in the bowing direction to an excitation of the second polarization. A Schelleng minimum bow-force plot was produced that looks similar to ones found in the literature, with the difference that this diagram was calculated for different notes being played on an instrument. This offered the opportunity to explore the note-by-note variation of minimum bow-force on the same instrument or over different instruments. The second polarization of the string was taken into account by allowing the string to vibrate in both polarizations and the bow-hair to vibrate in its transverse direction. The result was a general reduction in minimum bow-force with no obvious frequency dependence, and with a stronger effect when bowing the string farther from the bridge. Moreover, the longitudinal vibration of the bow-hair was added to the model and its effect in modulating the effective bow-speed was studied. A general reduction in minimum bow-force was observed, similar to the second string polarization case, and the occurrence of ALF notes was found to be much more frequent compared to the rigid bow case. Finally, the effect of the sympathetically tuned coupled strings was studied. A noticeable reduction in minimum bow-force was observed at *G3* which was the dominant wolf of the instrument before inclusion of the sympathetic strings. This effect and a minor reduction in *A3* were justified by harmonic relations between the played notes and the sympathetic strings. The results are not further pursued here as the main focus of this article was to describe the theoretical background and modeling procedure. The results will be further discussed and experimentally validated in future studies.

Acknowledgments

The authors would like to thank the Centre for Interdisciplinary Research in Music Media and Technology (CIRMMT) for partially support this project and making this collaboration possible. We thank two anonymous reviewers for detailed constructive comments. The first author is financially supported through a Richard H. Tomlinson doctoral fellowship to McGill University.

5. REFERENCES

[1] M. E. McIntyre and J. Woodhouse, "On the fundamentals of bowed string dynamics," *Acustica*, vol. 43, pp. 93-108, 1979.

[2] R. Pitteroff and J. Woodhouse, "Mechanics of the contact area between a violin bow and a string. Part II: Simulating the bowed string," *Acta Acustica united with Acustica*, vol. 84, pp. 744-757, 1998.

[3] J. Woodhouse, "Bowed string simulation using a thermal friction model," *Acta Acustica united with Acustica*, vol. 89, pp. 355-368, 2003.

[4] R. Pitteroff and J. Woodhouse, "Mechanics of the Contact Area Between a Violin Bow and a String. Part I: Reflection and Transmission Behaviour," *Acta Acustica united with Acustica*, vol. 84, pp. 543-562, 1998.

[5] J. C. Schelleng, "The bowed string and the player," *The Journal of the Acoustical Society of America*, vol. 53, pp. 26-41, 1973.

[6] L. Cremer, *The Physics of the Violin*. Cambridge MA: The MIT Press, 1984.

[7] J. Woodhouse and P. M. Galluzzo, "The bowed string as we know it today," *Acta Acustica united with Acustica*, vol. 90, pp. 579-589, 2004.

[8] J. Woodhouse and A. R. Loach, "Torsional behaviour of cello strings," *Acta Acustica united with Acustica*, vol. 85, pp. 734-740, 1999.

[9] J. Woodhouse, "On the playability of violins. Part I: Reflection functions," *Acustica*, vol. 78, pp. 125-136, 1993.

[10] F. Friedlander, "On the oscillations of the bowed string," in *Proc. Cambridge Philos. Soc*, 1953, p. 516.

[11] J. H. Smith and J. Woodhouse, "The tribology of rosin," *Journal of the Mechanics and Physics of Solids*, vol. 48, pp. 1633-1681, 2000.

[12] P. M. Galluzzo, "On the playability of stringed instruments," Ph. D. thesis, Trinity College, University of Cambridge, Cambridge, UK, 2003.

[13] J. Woodhouse and R. S. Langley, "Interpreting the Input Admittance of Violins and Guitars," *Acta Acustica united with Acustica*, vol. 98, pp. 611-628, 2012.

[14] J. Woodhouse, "On the synthesis of guitar plucks," *Acta Acustica united with Acustica*, vol. 90, pp. 928-944, 2004.

[15] A. Askenfelt, "Observations on the violin bow and the interaction with the string," in *Proceedings of the International Symposium on Musical Acoustics*, 1995.

[16] C. E. Gough, "Violin bow vibrations," *The Journal of the Acoustical Society of America*, vol. 131, p. 4152, 2012.

[17] H. Mansour, J. Woodhouse, and G. P. Scavone, "Time-domain simulation of the bowed cello string dual-polarization effect," in *Proceedings of the International Congress on Acoustics*, Montreal, Canada, 2013.

[18] K. Guettler, "Some typical properties of bowed strings," http://knutsacoustics.com/files/Typical-string-properties.pdf, last accessed, 2013.

[19] E. Schoonderwaldt, K. Guettler, and A. Askenfelt, "An empirical investigation of bow-force limits in the Schelleng diagram," *Acta Acustica united with Acustica*, vol. 94, pp. 604-622, 2008.

[20] R. J. Hanson, F. W. Halgedahl, and K. Guettler, "Anomalous low-pitched tones from a bowed violin string," *The Journal of the Acoustical Society of America*, vol. 97, pp. 3270-3270, 1995.

[21] C. V. Raman, "On the mechanical theory of vibrations of bowed strings," *Indian Assoc. Cult. Sci. Bull.*, vol. 15, pp. 243-276, 1918.

[22] J. Woodhouse, "On the playability of violins. Part II: Minimum bow force and transients," *Acustica*, vol. 78, pp. 137-153, 1993.

[23] K. Guettler, "On the creation of the Helmholtz motion in bowed strings," *Acta Acustica united with Acustica*, vol. 88, pp. 970-985, 2002.

[24] J. Reel, "Mari Kimura on Subharmonics," in *Strings*, June 2009.

[25] C. E. Gough, "The theory of string resonances on musical instruments," *Acustica*, vol. 49, pp. 124-141, 1981.